Thin Solid Films 528 (2013) 213–216

Contents lists available at SciVerse ScienceDirect

Thin Solid Films

journal homepage: www.elsevier.com/locate/tsf

Pseudocapacitive performance of vertical copper oxide nanoflakes

Z. Endut [a,*], M. Hamdi [a], W.J. Basirun [b]

[a] Centre of Advanced Manufacturing and Material Processing (AMMP), Department of Engineering Design and Manufacture, Faculty of Engineering, University of Malaya, 50603, Kuala Lumpur, Malaysia
[b] Department of Chemistry, Faculty of Science, University of Malaya, 50603, Kuala Lumpur, Malaysia

ARTICLE INFO

Available online 6 November 2012

Keywords:
Copper oxide
Supercapacitor
Nanoflakes

ABSTRACT

Vertical copper oxide (CuO) nanoflakes have been formed by oxidation in NaOH solution. Their structural, surface morphology and oxidation states were characterized using X-ray diffraction (XRD), field emission scanning electron microscopy (FESEM) and X-ray photoelectron spectroscopy (XPS) respectively. Pseudocapacitive behavior of CuO nanoflakes was investigated by cyclic voltammetry and constant current charge–discharge test. CuO nanoflakes were vertically grown with high lateral aspect ratio and consist of monoclinic lattice as shown by the presence of two peaks close to $2\theta = 35.6^{o}$ and 38.7^{o} in the XRD. Charge–discharge test gave a capacitance value of 190 F g^{-1} in 1.0 M KOH electrolyte at 2 mA cm^{-2} current density. The cycling test showed 67% stability after 2000 cycles and reduced specific capacitance from 190 F g^{-1} to 125 F g^{-1}. Specific capacitance of CuO nanoflakes is higher than 26.44 F g^{-1} of globular CuO at 2 mA cm^{-2} as reported in literature due to enhanced specific surface area.

1. Introduction

Supercapacitors are important electrical energy storage devices due to their high specific power density, fast recharge capabilities and long cycle life compared with batteries [1,2]. These devices have been used in many power source applications such as camera flash equipment, cellular phones and hybrid cars. In general, supercapacitors can be classified according to their storage mechanisms into electrical double layer capacitor (EDLC) and pseudocapacitors. The former is based on a non-faradaic reaction with accumulation of charges through electrostatic interaction at the electrode–electrolyte interface and the latter is based on a faradaic redox reaction on the surface of active materials [3,4].

It is important for pseudocapacitors to have high specific surface area, high electrical conductivity, and fast charge diffusion process in order to achieve high power densities and energy densities [5]. Hydrous ruthenium oxides (denoted as $RuO_x \cdot nH_2O$) with amorphous structure have been reported to be promising electrode materials for pseudocapacitor applications due to their intrinsically excellent quasi-metallic conductivity and high pseudocapacitance. However, the high cost of the compound has placed huge obstacles for its large scale manufacture [5–11]. Therefore, a lot of effort has been devoted to develop alternative pseudocapacitor electrode materials such as nickel oxide [6,7], cobalt oxide [8,9] and manganese oxide [10,11].

Due to its low cost, chemical stability and being environmentally-friendly, nanostructured copper oxides (CuO_x) have been synthesized using various methods such as electrodeposition [12], template-free growth [13], precipitation method [14] and chemical bath deposition [15] for supercapacitor applications. Nanostructured CuO with large surface area will improve specific capacitance of this material. For instances, cauliflower-like CuO exhibited a higher specific capacitance of 116.9 F g^{-1} compared with 26 F g^{-1} of globular CuO as found by Zhang et al. [14]. Meanwhile, Hsu et al. synthesized lotus-like CuO/$Cu(OH)_2$ array electrode which produced excellent specific capacitance of 278 F g^{-1} with capacitance loss of 15% over 5000 cycles [24]. CuO nanostructures have been also tested as Li ion battery anodes and have shown high Li-ion storage capacity, which suggests that CuO can offer high-charge storage capacity through a redox reaction [16,17]. Copper forms two well-known oxides: tenorite (CuO) and cuprite (Cu_2O). Both the tenorite and cuprite are *p*-type semiconductors having band gap energy of 1.21 to 1.51 eV and 2.10 to 2.60 eV respectively [27]. However, this gives low electrochemical capacitance due to its poor electrical conductivity. Hence, a profound understanding of copper oxide nanostructures is required before they can be utilized as supercapacitor electrodes.

The electrochemical behavior of Cu in aqueous solutions with different pH has been extensively studied [18,19]. Electrochemical dissolution of Cu occurs in acidic solutions. However, in neutral and alkaline solutions, surface passivation of Cu occur with the formation of $CuO/Cu(OH)_2$ bilayer when the applied potential is higher than a certain value [19]. In this study, the synthesis and characterization of porous copper oxide nanoflakes by simple chemical bath oxidation in alkaline solution [20] and its application as binder-free supercapacitor

* Corresponding author. Tel.: +60 3 7967 5382; fax: +60 3 7957 5330.
E-mail address: rg253c@yahoo.com (Z. Endut).

0040-6090/$ – see front matter.
http://dx.doi.org/10.1016/j.tsf.2012.09.084

electrode is investigated. The copper oxide film is characterized by field emission scanning electron microscopy (FESEM), X-ray photoelectron spectroscopy (XPS), X-ray diffraction (XRD) and cyclic voltammetry (CV) and galvanostatic charge–discharge testing.

2. Experimental procedures

The CuO nanoflakes were synthesized by surface oxidation of a Cu foil. The Cu foil was sonicated in a 3 M HCl aqueous solution for 15 min to remove any surface impurities and oxide layers on the Cu surface. The acid treated Cu foils were rinsed several times with ethanol and distilled water. Then the cleaned Cu foils were immersed in 30 mM NaOH solution at 75 °C for 12 h, washed several times with distilled water and dried at 100 °C in air for 1 h. A uniform black colored copper oxide film was finally obtained which was distinguishable from the Cu foils.

Scanning electron micrographs were taken using a JEOL JSM-840A Field Emission Scanning Electron Microscope (FESEM) with an operating voltage of 5 kV. The phase detection of CuO nanoflakes was determined by X-ray diffraction (XRD) (Siemens D5000, with a Cu-Kα radiation source mounted on a horizontal θ–2θ goniometer). The X-ray photoelectron spectroscopy (XPS) analysis of CuO nanoflakes was performed using XPS Axis Ultra from Kratos equipped with monochromatic Al Kα radiation (BE = 1486.6 eV). The sample was analyzed inside an analysis chamber pressure of about 1×10^{-10} Pa. To correct possible deviations caused by electric charge of the samples, the C 1 s peak of carbon at 284.5 eV was taken as the internal standard or reference. Cyclic voltammetry and charge–discharge measurements were carried out using a potentiostat/galvanostat model PGSTAT-302N from Autolab (The Netherlands, distributed by Metrohm Malaysia), controlled by a USB_IF030 interface card and GPES software installed in a computer. The experiments were performed in a three electrode electrochemical cell containing 1 M KOH aqueous solution as the electrolyte at room temperature, with Hg/HgO as the reference electrode and Pt wire as the counter electrode. The scan rates were from 5 mV s^{-1} to 60 mV s^{-1} between 0 V and −0.6 V while constant current of 2 mA and 5 mA were used in the charge–discharge experiments. The as-prepared CuO nanoflake film used as the binder-free working electrode had nominal surface area of 4 cm^2. The weight of the CuO nanoflakes was obtained by dissolving CuO in 6 M HCl. The obtained electrode has a CuO loading of 0.23 mg which will be used in calculating specific capacitance.

3. Results and discussions

3.1. Surface morphology

Fig. 1a is the FESEM image of the copper oxide nanoflake surface on the Cu substrate. Under low magnification, the Cu substrate can be seen fully covered by a homogeneous and uniform film. Fig. 1b is a higher magnification of the nanoflake image which shows that the nanoflake structures are well adherent and vertically grown on the Cu substrate. The lateral size and thickness of the nanoflakes are estimated to be around 600 and 20 nm respectively, and indicates a high lateral aspect ratio. These nanoflakes are interconnected with each other and create pores and crevices which allow large surface area for easy diffusion of the electrolyte onto the nanoflake surface.

3.2. Phase detection

XRD technique allows the determination of the chemical identity and the crystallographic orientation of the black copper oxide film. Fig. 2 shows the diffractogram of the copper oxide film together with the lattice planes of the copper oxide peaks. The XRD pattern shows the presence of two peaks close to $2\theta = 35.6^{o}$ and 38.7^{o} which correspond to the ($\bar{1}11$) and (111) respectively for the tenorite with a monoclinic lattice for CuO (JCPDS No. 80-0076) [19]. The other two strong peaks are attributed to the bulk copper (face centered cubic lattice) from the underlying copper substrate.

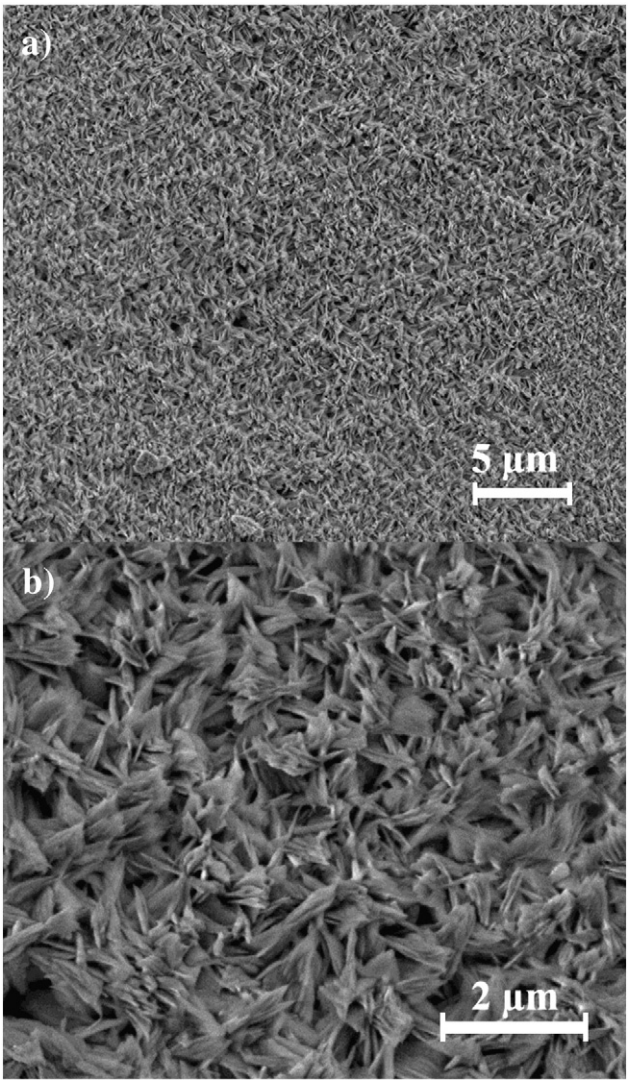

Fig. 1. FESEM micrographs of copper oxide nanoflakes. (a) Lower magnification, (b) higher magnification.

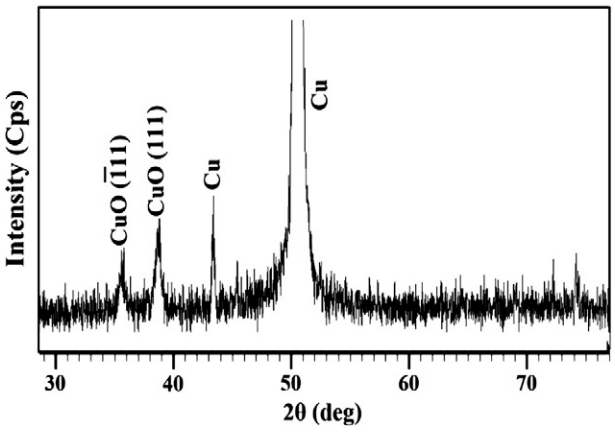

Fig. 2. XRD pattern of copper oxide nanoflakes.

3.3. Chemical composition

To further confirm the identity of the copper oxide film, XPS analysis was used to determine oxidation state of the Cu. All the binding energies obtained in the XPS analysis are calibrated using the C 1 s peak with a binding energy of 284.5 eV as the reference and deconvoluted by using Shirley background. The CuO characteristics can be identified by using the binding energy peak value, the existence of satellite pattern and the binding energy peak gap between Cu $2p_{3/2}$ and Cu $_{2p1/2}$. As shown in Fig. 3, the peak at 933.4 eV with high intensity is attributed to Cu $2p_{3/2}$ while the peaks at 953.3 eV are attributed to Cu $2p_{1/2}$. The binding energy peak at 933.4 eV belongs to CuO [20]. Furthermore, the gap between the Cu $2p_{3/2}$ and $2p_{1/2}$ is around 19.9 eV, which is in good agreement with the standard value of 19.9 eV for CuO. In addition to the Cu $2p_{3/2}$ and $2p_{1/2}$ peaks, typical CuO-satellite peaks appear at binding energies of 943.8 and 963.7 eV, and the existence of a strong satellite pattern for the Cu 2p rules out the possibility of the presence of Cu_2O phase. Since the 3*d* shell is expected to be completely filled in Cu_2O, the shake up satellite peaks indicate the presence of an unfilled Cu 3*d*9 shell, that is, the existence of CuO at the surface [21,22]. It has been also reported that Cu_2O can be easily covered by a relatively more stable CuO surface layer [24]. Another Cu $2p_{3/2}$ peak at 935.7 eV with low intensity is attributed to $Cu(OH)_2$ [26]. Thus, the XRD and XPS results support the conclusion that the nanostructures are composed mainly of CuO. The CuO formation can be described with the following mechanism. With a low concentration of 30 mM NaOH, the dissolution rate of Cu becomes slow and a dark film (the duplex $CuO/Cu(OH)_2$ passivation layer) is slowly formed on the surface of the Cu electrode. Applying heat to the solution for about 12 h transforms the $Cu(OH)_2$ to black CuO.

3.4. Electrochemical capacitance

The electrochemical performance of the CuO nanoflake film is measured using cyclic voltammetry and galvanostatic charge–discharge experiments. A pair of cathodic and anodic peaks is clearly observed in the CV in Fig. 4 which indicates that the capacitance characteristics are mainly governed by faradaic redox reactions on the nanoflake surface. The peak potentials shift to more anodic and cathodic directions with the increase of scan rate but the shifting can be seen clearly only at 20 mV s^{-1} scan rate and below suggesting pseudocapacitance behavior with limited performance [13]. Furthermore, the peak current increment with scan rate from 5 mV s^{-1} to 60 mV s^{-1} shows a non-linear relationship indicating reversibility

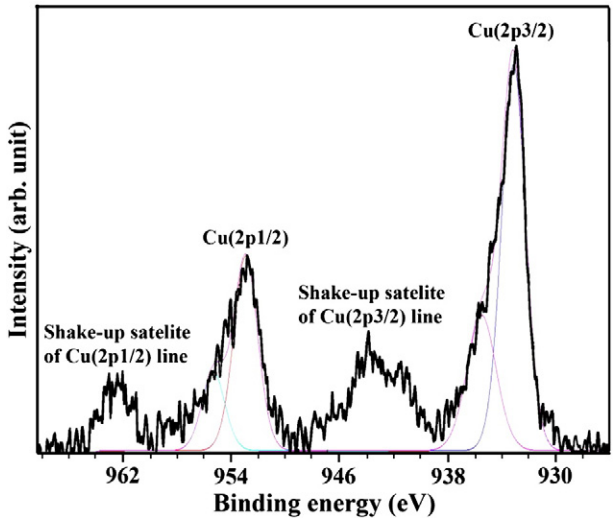

Fig. 3. The XPS spectrum of the Cu(2p) core level of the copper oxide nanoflakes (thick line). The fitted curves are shown under the spectrum (thin line).

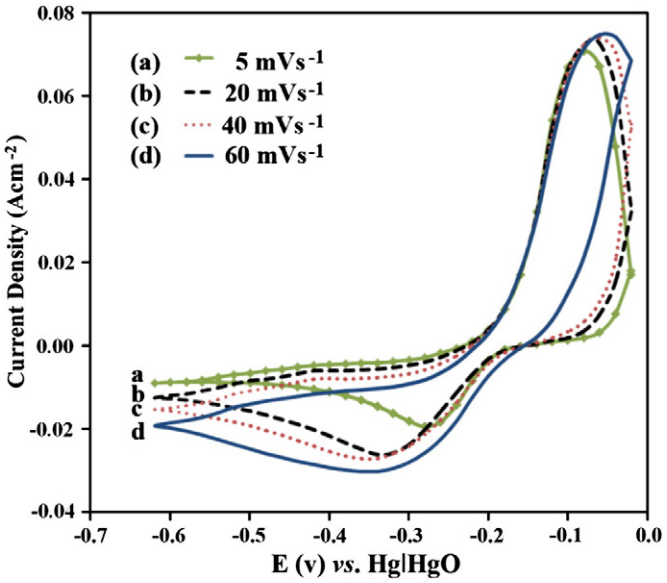

Fig. 4. Cyclic voltammograms of the as-prepared copper oxide nanoflakes electrode in 1 M KOH electrolyte.

issue. The large peak potential separation between anodic and cathodic is likely related with the low electronic conductivity of CuO nanoflakes [25]. From the CV reports of CuO in alkaline electrolytes [13], the following redox reactions are involved in the transition between Cu(I) and Cu(II) species.

$$Cu_2O + 2OH- \Longleftrightarrow 2CuO + H_2O + 2e^- \quad (1)$$

The anodic peak A in Fig. 4 is attributed to the oxidation of Cu_2O to CuO (Eq. (1)). The cathodic peak B can be ascribed to the reduction of CuO (Eq. (1)) to Cu_2O. The reduction of CuO to Cu and the oxidation of CuO to Cu(III) species (such as Cu_2O_3) are unlikely to occur in the potential range of this study [23]. Nevertheless, it can be concluded that the capacitance of CuO originates from the redox reaction of Cu(I)/Cu(II) couple. It should be pointed out that the CVs shown in Fig. 4 are the stabilized curves after 5 potential cycles, during which CuO originally formed on copper electrode was partially reduced to Cu_2O.

Fig. 5 shows the charge–discharge profile for the CuO nanoflakes from 0 to −0.6 V with a current density of 2 mA and 5 mA. The specific capacitance is calculated according to the following equation:

$$C = \frac{I\Delta t}{A\Delta V} \quad (2)$$

where C (F cm^{-2}) is the specific capacitance, I (mA) is the discharge current, A (cm^2) is the nominal surface area, ΔV (V) and Δt (s) represent the potential drop during discharge and total discharge time respectively. The CuO nanoflakes with monoclinic phase give pseudocapacitance values of 175 mF cm^{-2} at 2 mA and 153 mF cm^{-2} at 5 mA in 1 M KOH electrolyte. For this value, the normalized specific capacitance based on 0.23 mg active CuO and 4 cm^2 active areas are 190 F g^{-1} at 2 mA and 166.75 F g^{-1} at 5 mA. The significant capacitance decrease resulting from the increase of discharge current density is likely caused by the increase of potential drop due to electrode resistance and the relatively low utilization of the active material under higher discharge current densities [24,25].

Fig. 6 shows the cyclability of these CuO nanoflakes using galvanostatic charge–discharge testing over 2000 cycles at a current density of 2 mA cm^{-2} within the potential range of 0–0.6 V. The 67% stability is retained after 2000 cycles. The specific capacitance values are decreased by a large amount within the first 100 cycles due to the loss of active material caused by dissolution and/or detachment

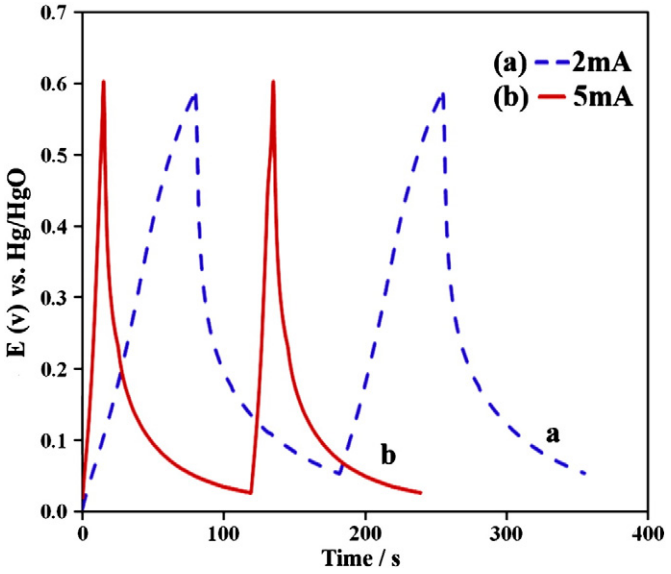

Fig. 5. Galvanostatic charge–discharge of copper oxide nanoflakes with different currents: (a) 2 mA, (b) 5 mA.

during the early charging/discharging cycles in the electrolyte and irreversible electrode reaction during the early cycles. After 2000 cycles, the specific capacitance reduced from 190 F g^{-1} to 125 F g^{-1}. However, this specific capacitance is still higher than that of the CuO multilayer nanosheets prepared by Lokhande et al. which showed a specific capacitance of 43 F g^{-1} in Na_2SO_4 electrolytes [12,15]. The redox electrolyte used in this study contributes to higher specific capacitance due to surface redox. However, our capacitance value is inferior to that of the lotus-like copper oxide obtained by Hsu et al. which showed a specific capacitance of 278 F g^{-1} with only 15% loss after 5000 cycles [24]. In addition, the capacitance loss of their materials also occurred in early stage of cycling test. Poor capacitance retention during cycling due to the destruction of the CuO crystal structure during the ion insertion–extraction process can also occur [16,17].

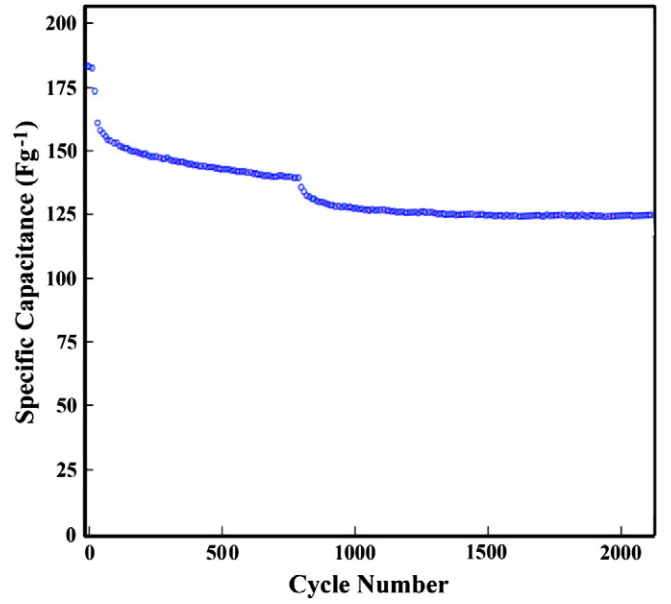

Fig. 6. Cyclability test of copper oxide nanoflakes at a current density of 2 mA cm^{-2}.

4. Conclusions

In summary, we demonstrated a simple method to produce binder-free CuO nanoflakes by chemical oxidation in 30 mM NaOH solution at 70 °C for about 12 h. At high magnification the black copper oxide FESEM micrographs show that the nanoflakes have vertical orientation which creates pores and crevices between them. XPS and XRD analysis confirmed the oxidation state of this CuO. Cyclic voltammetry show redox peaks at anodic and cathodic scans which are mainly from the oxidation and reduction of CuO to Cu_2O. The CVs suggest that irreversible pseudocapacitance occurred at the early stage, thus limiting its performance as shown in non-linear relationship behavior of peak currents with scan rate. The cycling test showed 67% stability after 2000 cycles and reduced specific capacitance from 190 F g^{-1} to 125 F g^{-1}. However, the specific capacitance value of 190 F g^{-1} is still comparatively higher than the specific capacitance reported in some literature and this simple and cost-saving process makes this CuO nanoflake a promising method to produce binder-free supercapacitor electrodes.

Acknowledgments

The authors would like to acknowledge financial support from Postgraduates Fund (PV058/2011A) from Institute of Research Management and Monitoring (IPPP) and High Impact Research (HIR-MOHE-D000001-16001), University of Malaya and MyPhD programs, Ministry of Higher Education (MOHE), Malaysia.

References

[1] B.E. Conway, J. Electrochem. Soc. 138 (1991) 1539.
[2] R. Kotz, M. Carlen, Electrochim. Acta 45 (2000) 2483.
[3] E. Frackowiak, F. Beguin, Carbon 40 (2002) 1775.
[4] Y.G. Wang, X.G. Zhang, Electrochim. Acta 49 (2004) 1957.
[5] C.D. Lokhande, D.P. Dubal, O.-S. Joo, Curr. Appl. Phys. 11 (2011) 255.
[6] K.-W. Nam, K.-B. Kim, J. Electrochem. Soc. 149 (2002) A346.
[7] K.R. Prasad, N. Miura, Appl. Phys. Lett. 85 (2004) 4199.
[8] C. Lin, J.A. Ritter, B.N. Popov, J. Electrochem. Soc. 145 (1998) 4097.
[9] V. Srinivasan, J.W. Weidner, J. Power Sources 108 (2002) 15.
[10] C.-C. Hu, T.-W. Tsou, Electrochem. Commun. 4 (2002) 105.
[11] R.N. Reddy, R.G. Reddy, J. Power Sources 124 (2003).
[12] V.D. Patake, S.S. Joshi, C.D. Lokhande, O.-S. Joo, Mater. Chem. Phys. 114 (2009) 6.
[13] G. Wang, J. Huang, S. Chen, Y. Gao, D. Cao, J. Power Sources 196 (2011) 5756.
[14] H. Zhang, J. Feng, M. Zhang, Mater. Res. Bull. 43 (2008) 3221.
[15] D.P. Dubal, D.S. Dhawale, R.R. Salunkhe, V.S. Jamdade, C.D. Lokhande, J. Alloys Compd. 492 (2010) 26.
[16] J.C. Park, J. Kim, H. Kwon, H. Song, Adv. Mater. 21 (2009) 803.
[17] X. Zhang, W. Shi, J. Zhu, D.J. Kharistal, W. Zhao, B.S. Lalia, H.H. Hng, Q. Yan, ACS Nano 5 (2011) 2013.
[18] H.J. Qiu, L. Lu, L.Y. Xue, X.R. Huang, Electrochim. Acta 55 (2010) 6081.
[19] L. Lu, X. Huang, Microchim. Acta 175 (2011) 151.
[20] O. Akhavan, E. Ghaderi, J. Mater. Chem. 21 (2011) 12935.
[21] S. Sahoo, S. Husale, B. Colwill, T.M. Lu, S. Nayak, P.M. Ajayan, ACS Nano 3 (2009) 3935.
[22] T. Dong, C. Chen, H. Cheng, C. Chen, N. Jheng, Inorg. Chim. Acta 367 (2011) 158.
[23] S. Nakayama, A. Kimura, M. Shibata, S. Kuwabata, T. Osakai, J. Electrochem. Soc. 148 (2001) B467.
[24] Y.K. Hsu, Y.C. Chen, Y.G. Lin, J. Electroanal. Anal. 673 (2012) 43.
[25] J. Huang, J. Zhu, K. Chen, Y. Xu, D. Cao, G. Wang, Electrochim. Acta 75 (2012) 273.
[26] G. Lavareda, C.N. Carvalho, A.M. Ferraria, A.M. Botelho, A. Amaral, J. Nanosci. Nanotechnol. 12 (2012) 1.
[27] A. Chen, H. Long, X. Li, Y. Li, G. Yang, P. Lu, Vacuum 83 (2009) 927.